

Interaction between cell membranes and protein inclusions in the large-deformation regime

Gaetano Ferraro^{1, 2, 3} and Michele Castellana^{1, 2, *}

¹*Institut Curie, PSL Research University, Paris, France*

²*CNRS UMR168, 11 rue Pierre et Marie Curie, 75005, Paris, France*

³*Polytechnic University of Turin, Corso Castelfidardo 39, 10129 Turin, Italy*

(Dated: January 23, 2026)

Biological membranes are dynamic surfaces whose shape and function are critically influenced by protein inclusions (PIs). While membrane deformations induced by PIs have been extensively studied in the small-deformation regime, a variety of processes involves strong membrane deformations. We investigate the interaction between lipid membranes and PIs in the large deformation (LD) regime, with the finite-element method. We develop an approximate analytical solution that captures key features of the LD regime. We show that the force exerted by the membrane on a PI displays non-monotonic behavior with respect to the PI vertical displacement. The qualitative features of this force appear to be independent of the protein geometry. For two interacting PIs, the membrane-mediated potential exhibits sub-power-law decay with inter-protein distance, reflecting the complex nature of the elastic medium. The interaction potential shows that conical PIs with identical and opposite orientations repel and attract, respectively, confirming the analogy between PI orientation and electric charge, in the LD regime. In the presence of membrane flows, we identify a characteristic velocity that separates two regimes in which bending rigidity and viscous effects dominate, respectively, implying the onset of flow-induced deformations above such velocity threshold. Overall, our results provide quantitative predictions for membrane-protein systems in biologically relevant scenarios involving LDs, with implications for protein sorting, clustering, and membrane trafficking.

I. INTRODUCTION

Biological membranes are dynamic and deformable surfaces whose shape and function are critically influenced by the presence of protein inclusions (PIs) [1, 2]. Such PIs often impose geometric constraints, e.g., contact angles between the protein and the membrane, or membrane displacement, that drive local membrane deformations [3] and may govern membrane-mediated interactions [4]. Understanding how these deformations arise and interact is central to elucidate key biological processes, such as cell-shape regulation and protein sorting [5].

Membrane deformations induced by PIs have been the subject of numerous investigations [6]. From the modelling standpoint, they may be described by the shape equation [7–9], whose variational formulation stems from the free energy originally proposed by Helfrich [10]. Studies on such membrane deformations in the literature focus on the small deformation (SD) regime [11–14], and rely on perturbative expansions about the flat-membrane configurations.

However, a wide variety of physical situations may fall beyond the SD scenario. For instance, a PI moving at large enough velocities may induce a strong membrane invagination. Also, multiple PIs positioned close enough to each other, may induce strong membrane deformations and gradients which cannot be described as SDs.

In this work, we explore the interaction between a lipid membrane and a PI, in the large deformation (LD) regime, leveraging the finite element (FE) method to solve the problem numerically. We then focus on the features resulting from this solution, such as the membrane shape, flows, the membrane-mediated interaction between two PIs, and others, and discuss their physical interpretation.

The paper is structured as follows. In Section II we discuss the state of the art on membrane-mediated forces. Section III contains our results in the LD regime. In particular, in Section III A we focus on the steady state in the absence of flows. After discussing the limitations of the SD solution in Section III A 1, in Section III A 2 we present an approximate, analytical solution for the LD regime. In Section III A 3 we discuss the force exerted by the membrane on the PI, and in Section III A 4 the membrane-mediated interaction between a pair of PIs. In Section III B we study the steady state

* Corresponding author: michele.castellana@curie.fr

in the presence of flows by focusing on the effect of inflow velocity on membrane shape. Finally, Section IV is devoted to the discussion and interpretation of the results.

II. STATE OF THE ART

On top of numerous experimental studies—see for example [3, 4, 15]—membrane-mediated forces between proteins have been subject of interest and research in the past few decades from the theoretical standpoint. However, the existing theoretical studies are restricted to SDs—see below. In the pioneering study of Goulian et al., a power-law interaction between protein inclusions has been found in the SD limit [11], and later on studied for conical inclusions, in the SD regime, as a function of lateral membrane tension [12] and of the inclusion contact angle [13]. Studies with more than two inclusions showed, for SDs, the presence of non-pairwise forces between the inclusions, which allow for the formation of membrane-bound protein aggregates [14]. In addition, the power-law dependence on inclusion symmetries was studied in the SD limit [16]. The nature of this interaction was then studied, in the SD regime, as function of the ‘hardness’ of the protein-protein interaction potential [17]. A geometrical approach has been recently proposed and used to derive force-distance relations in the SD regime [18]. Expressions for the inter-particle forces, not restricted to SDs, have been derived by leveraging the system symmetries [19], but they lack quantitative predictive power in the LD regime due to the absence of a full numerical solution. Finally, studies which go beyond the SD regime do exist, but they are limited to the analysis of membrane vesicles [20] or tubes [8], both neglecting finite size of the proteins.

Regarding the effect of membrane flows on membrane shape, Arroyo and DeSimone [21] showed that membrane viscosity plays a crucial role in the relaxation dynamics of fluid membranes, highlighting the importance of viscous effects in dynamical models. In [22], coupled mean-field equations describing the time evolution of protein density and membrane shape were derived, accounting for the interplay between curvature elasticity and transport processes. Finally, in [23], a FE method for fluid membranes was developed and applied to the simulation of dynamical prolate-to-oblate transitions of simplified red blood cells under optical tweezing.

Parameter	Description	Value
r_0	Protein radius	10 nm
η	Viscosity	10^{-8} Pa m sec
σ_0	Surface tension	10^{-6} N/m
κ	Bending rigidity	$10 k_B T$
T	Temperature	300 K

TABLE I: Parameters for a lipidic cell membrane [32–37].

III. RESULTS

A. Steady state with no flows

In this Section, we will present the results for a biological membrane at steady state with no flows, in a given surface-tension gradient. Because the presence of surface-tension gradients would imply the presence of flows, here we will consider constant surface-tension profiles, where the value of the surface tension is given by experimental data [24]. We describe the membrane shape by using the Monge gauge [25, 26]: The membrane surface is a two-dimensional manifold embedded in three dimensions, described by a function $z(\mathbf{x})$, where $\mathbf{x} = (x^1, x^2)$ are the manifold coordinates, which are defined in a two-dimensional domain Ω , see for example Figs. 1 and 9. Given the tangent vectors to the coordinate lines $\mathbf{e}_1 \equiv (1, 0, \partial_1 z)$, $\mathbf{e}_2 \equiv (0, 1, \partial_2 z)$, the metric tensor is $g_{ij} = \mathbf{e}_i \cdot \mathbf{e}_j$ [27]. The membrane shape is determined by the shape equation [7–9]

$$\nabla^i \nabla_i H + 2H(H^2 - K) - H \frac{\sigma}{\kappa} = 0. \quad (1)$$

In Eq. (1), ∇ is the covariant derivative associated to the Levi-Civita connection induced by g , H and K the mean and Gaussian curvature, see [26, 28] for details. Also, κ is the bending rigidity and σ the surface tension [26].

Equation (1) is known to present the characteristic length

$$\ell \equiv \sqrt{\frac{\kappa}{\sigma}}. \quad (2)$$

For lengths smaller and larger than ℓ , the bending rigidity and the surface tension dominate the physical behavior of the system, respectively [29]. Given the parameter values of Table I, ℓ is around $20 r_0$, where r_0 is the radius of the PI [30, 31].

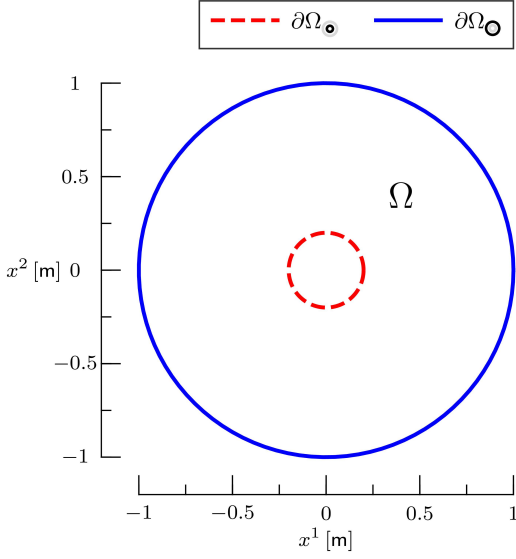


FIG. 1: Sketch of the domain Ω and its boundaries for the radially symmetric steady state of a membrane and protein inclusion, in the absence of flows. The center of $\partial\Omega_0$ (red dashed circle) is located at $x^1 = x^2 = 0$, and its radius is denoted by r_0 . The center of $\partial\Omega_0$ (blue solid circle) is located in the same position, and its radius is denoted by R .

1. Linearized equation

Equation (1) can be simplified in the case of a circular inclusion. Indeed, if the membrane shape is radially symmetric, Eq. (1) reduces to an ordinary differential equation (ODE). Moreover, Eq. (1) can be linearized for small values of

$$\omega \equiv \frac{\partial z}{\partial r}, \quad (3)$$

and it reduces to [38]

$$\left(1 - \frac{r^2}{\ell^2}\right)\omega - r\left(1 + \frac{r^2}{\ell^2}\right)\frac{d\omega}{dr} + 2r^2\frac{d^2\omega}{dr^2} + r^3\frac{d^3\omega}{dr^3} = 0. \quad (4)$$

Equation (4) has been extensively studied in the literature. However, its validity is limited to certain conditions: In the following, we assess these limitations by comparing its predictions with numerical solutions. To achieve this, we consider the

boundary conditions (BCs), see Fig. 1:

$$z = h_0 \quad \text{on } \partial\Omega_0 (r = r_0), \quad (5)$$

$$z = 0 \quad \text{on } \partial\Omega_0 (r = R), \quad (6)$$

$$n^i \nabla_i z = -\tan \alpha \quad \text{on } \partial\Omega_0 (r = r_0), \quad (7)$$

$$n^i \nabla_i z = 0 \quad \text{on } \partial\Omega_0 (r = R). \quad (8)$$

where n^i is the unit normal, which lies in the membrane tangent bundle and points outside the membrane manifold [28]. Equations (5) to (8) correspond to a membrane pinned on both boundaries $\partial\Omega_0$ and $\partial\Omega_0$. The protein is displaced vertically at an height equal to h_0 and the contact angle α is constrained at the protein boundary $\partial\Omega_0$ [8]. Such contact angle may reflect the angular span of the hydrophilic region of the PI, and it may depend on the membrane lipidic composition [15].

To assess the regime of validity of the linearized equation, we compared membrane profiles from FE solutions with the solution of Eq. (4). Figure 2 shows that the linear solution remains accurate for imposed contact angles of up to approximately $\tan \alpha \simeq 0.4$. For larger values of the contact angle, the linear approximation fails to capture the correct shape of the membrane and full non-linear equation (1) must be solved.

In what follows, we will focus on this regime, which is characterized by the presence of large gradients $\omega \gg 1$. The PI displacement and contact angle may have the same or opposite sign, leading to distinct deformation responses; these two situations are presented in Fig. 3.

2. Solution with zero mean curvature

Analytical insights about the LD regime for the membrane can be obtained considering the following approximate solution.

In order to simplify the equation, it is convenient to introduce the quantity ψ , by the relation

$$\omega = \frac{\psi}{\sqrt{1 - \psi^2}}. \quad (9)$$

In Section A, we show all geometrical quantities expressed in terms of ψ and its derivatives. Substi-

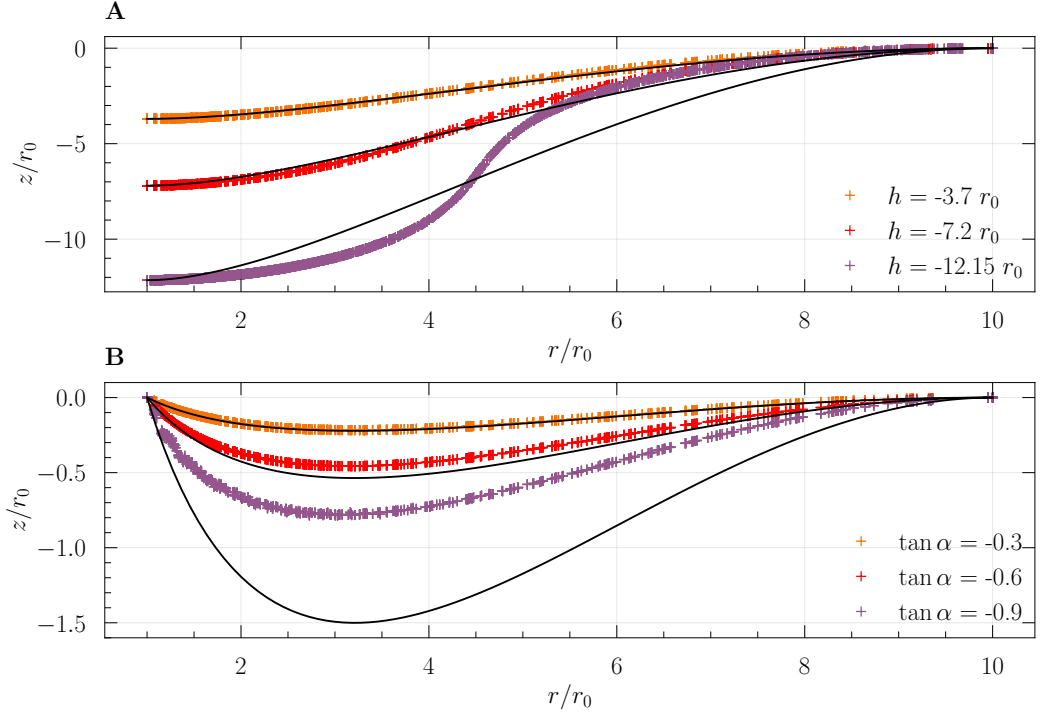


FIG. 2: Comparison between analytical and numerical membrane shapes obtained with fluid layer finite element software (IRENE) [28]. **A)** Comparison for fixed contact angle and different values of the protein vertical displacement h , with boundary conditions (5) to (8). **B)** Same as **A**, with fixed protein displacement and different values of the contact angle α .

tuting Eq. (A1) in Eq. (1), we obtain:

$$(1 - \psi^2) \frac{\partial^2 H}{\partial r^2} + \left(\frac{1 - \psi^2}{r} - \psi \frac{\partial \psi}{\partial r} \right) \frac{\partial H}{\partial r} + \left(\frac{2\psi}{r} \frac{\partial \psi}{\partial r} + \frac{1}{\ell} - 2H^2 \right) H = 0, \quad (10)$$

$$H = \frac{\partial \psi}{\partial r} + \frac{\psi}{r}. \quad (11)$$

Equation (11) admits a solution with zero mean curvature, of the form

$$\psi = \frac{C_1}{r}. \quad (12)$$

We observe that the two terms in the right-hand side of Eq. (11) are, respectively, the radial and angular curvature [27]. As a result, solution (12) does not imply that z is linear in r , i.e., that the radial curvature vanishes, but that the algebraic sum of radial and angular curvature is zero.

Although this solution is only valid for zero mean curvature, it constitutes an approximation of the exact solution in the general case where curvature is not zero. However, it allows for explicit, simple expressions of the membrane shape and height,

which may be useful on a qualitative level. In particular, here we infer a relation between the contact angle α and the corresponding spontaneous displacement of the protein. Indeed, substituting Eq. (12) in Eq. (9), and integrating, we obtain that the corresponding profile of the membrane is:

$$z(r) = -C_1 \ln \left(r - \sqrt{r^2 - C_1^2} \right) + C_2. \quad (13)$$

The integration constants C_1 and C_2 can be determined from the BCs (5) and (7), leading to:

$$z(r) = -r_0 \sin \alpha \ln \frac{r - \sqrt{r^2 - r_0^2 \sin^2 \alpha}}{R - \sqrt{R^2 - r_0^2 \sin^2 \alpha}}. \quad (14)$$

The displacement of the protein is then given by:

$$h = -r_0 \sin \alpha \ln \frac{r_0 - r_0 \sqrt{1 - \sin^2 \alpha}}{R - \sqrt{R^2 - r_0^2 \sin^2 \alpha}}, \quad (15)$$

For $R \gg r_0$, Eq. (15) becomes

$$h \simeq -r_0 \sin \alpha \left[\ln \frac{r_0}{R} + \ln (1 - \cos \alpha) \right] \quad (16)$$

The comparison between the numerical solution obtained with IRENE and the zero-mean-curvature

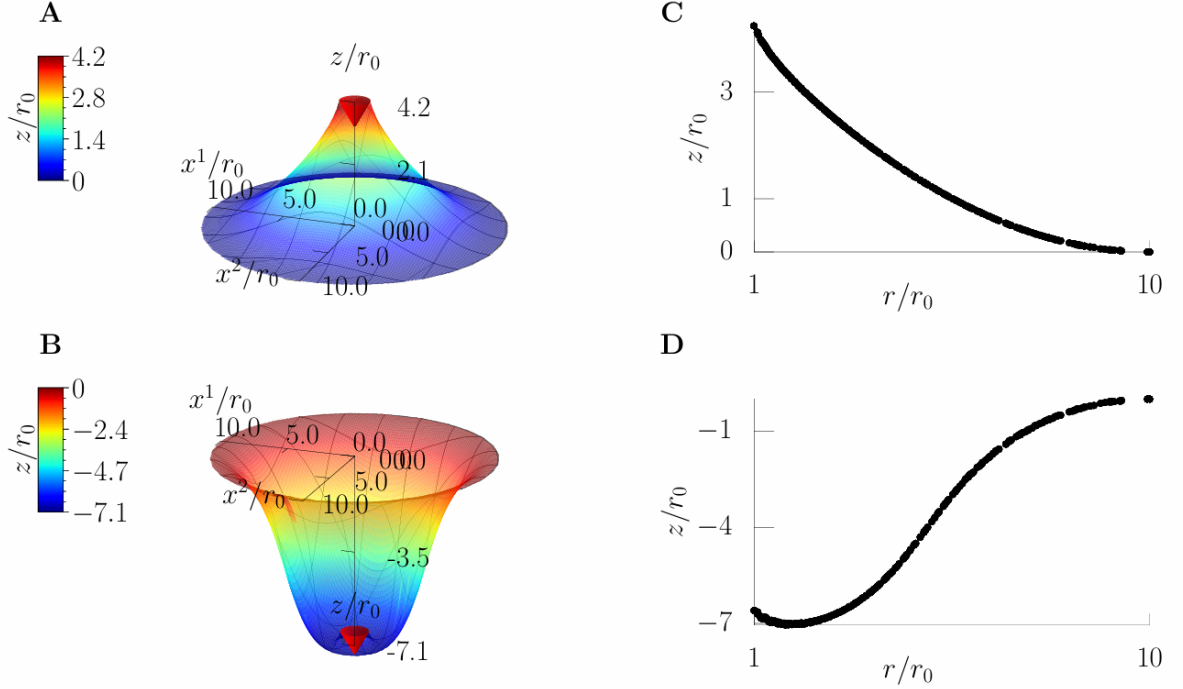


FIG. 3: Membrane shapes in the large-deformation regime, obtained with the fluid layer finite-element software (IRENE) [28]. **A)** Membrane deformation induced by a positive vertical displacement of the protein and positive contact angle, $h_0 = 4.2 r_0$ and $\tan \alpha = 0.5$, cf. Fig. 1. **B)** Membrane deformation induced by a negative vertical displacement of the protein and positive contact angle, $h_0 = -6.5 r_0$, $\tan \alpha = 0.5$, cf. Fig. 1. The corresponding membrane profiles are shown in panels **C**) and **D**), respectively. A convergence analysis of such type of radially symmetric solution with respect to the finite-element mesh resolution is reported in [28].

solution (14) is shown in Fig. 4. The Figure shows that the zero-mean-curvature solution yields a reasonable approximation for the numerically exact solution, see Section IV.

3. Forces

Another important feature in the interaction between the protein and the membrane is the force exerted by the membrane on the PI boundary. The expression for this force is derived in Section B, and its tangential and normal components read

$$\mathbf{f}_\perp = 2\kappa n^i \nabla_i H \quad (17)$$

$$= -2\kappa \frac{\partial H}{\partial r},$$

$$\mathbf{f}_\parallel = -n^i (2\kappa H^2 + \sigma) \mathbf{e}_i \quad (18)$$

In the LD regime, the force exerted by the membrane on the protein has been evaluated numerically with IRENE; results are shown in Fig. 5.

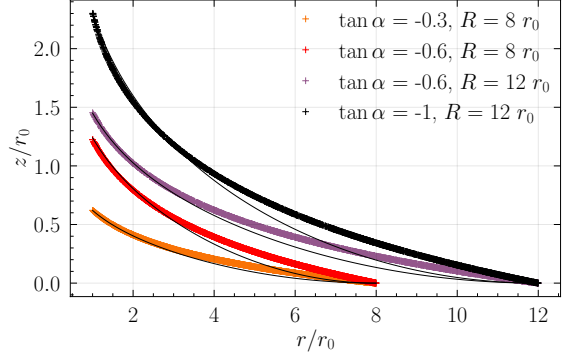


FIG. 4: Comparison between the solution with zero mean curvature (14) and the numerically exact, finite element (FE) solution, in the large-deformation regime. The FE solution (thin black curves) has been obtained with the fluid layer finite-element software (IRENE) [28], and the zero-mean-curvature solution is shown as thick colored curves. Both solutions are shown for different values of the membrane radius R and contact angle α .

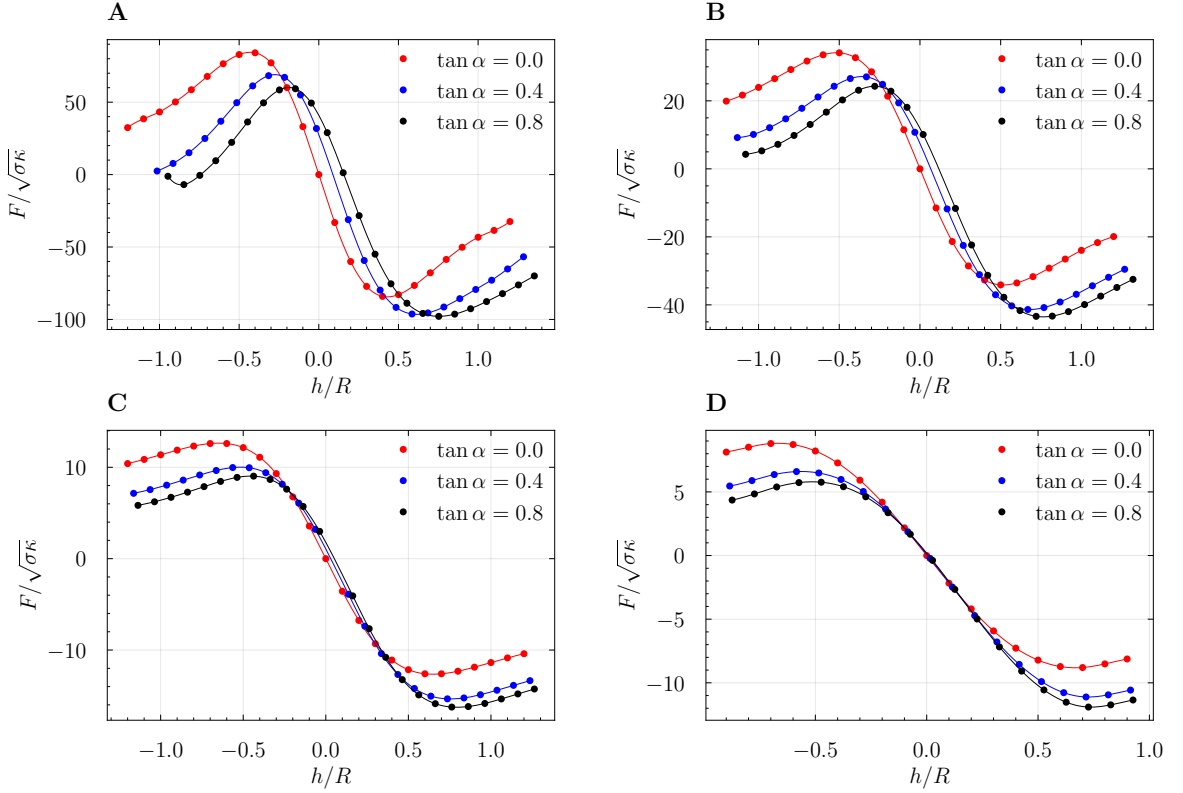


FIG. 5: Force exerted by the membrane on a protein inclusion along the z -axis, in the large-deformation regime. The force has been computed numerically by using the fluidIId layeR finiteE-Element softwaRe (IRENE) [28]. Different panels show the force as a function of the membrane vertical displacement h , for different values of the size R of the membrane domain. **A)** $R = 5 r_0$, **B)** $R = 10 r_0$, **C)** $R = 30 r_0$, **D)** $R = 100 r_0$.

4. Potential energy in a system with two proteins

In what follows, we will focus on the membrane-mediated interaction between the two **PIs**. We consider a square domain Ω with side L , containing two circular holes, which represent the two **PIs**, see Fig. 6.

In this case, the rotational symmetry of Fig. 1 no longer holds. As a result, the partial differential equation (PDE) (1) cannot be reduced to an **ODE**, and the analytical treatment of the problem is out of reach; we will thus study the solution numerically.

The centers of the two holes $\partial\Omega_{\bullet 1}$, $\partial\Omega_{\bullet 2}$ are located, respectively, at $\mathbf{c}_1 = (L/2 - d/2 - r_0, L/2)$ and $\mathbf{c}_2 = (L/2 + d/2 + r_0, L/2)$. Here, d is the distance between the two closest points on $\partial\Omega_{\bullet 1}$ and $\partial\Omega_{\bullet 2}$, and both **PIs** have radius r_0 , see Fig. 6.

We impose the following **BCs**:

$$z = 0 \text{ on } \partial\Omega_{\square}, \quad (19)$$

$$\nabla_i z = -\tan \alpha \hat{r}_i \text{ on } \partial\Omega_{\bullet^{1(2)}}, \quad (20)$$

$$n^i \nabla_i z = 0 \text{ on } \partial\Omega_{\square}, \quad (21)$$

where \hat{r} is the unit radius in the $x^1 x^2$ plane relative to the center of each **PI**.

For $d \gg \ell$, the deformation induced by a single **PI** decays exponentially with d , and so does the interaction [39]. On the other hand, when the distance between **PIs** is of the order of the protein dimension r_0 , also the tilt of the phospholipids must be taken into account [40]. Given that the phospholipid tilt is not currently described by our model, in what follows we will assume the interprotein distance to be larger than the **PI** radius, r_0 . To this end, we numerically compute the energy of the system [10] over a domain Ω containing two

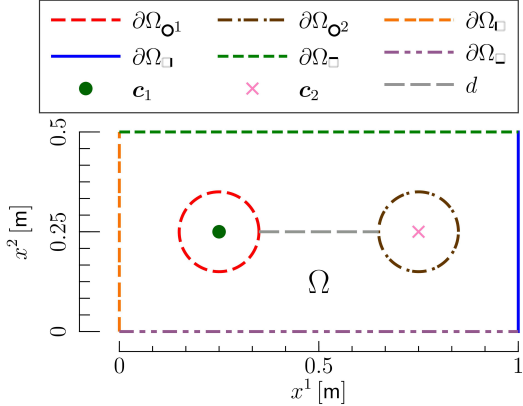


FIG. 6: Sketch of the domain Ω and its boundaries for the steady state of a membrane with two **PIs**, in the absence of flows. The domain size is $0 \leq x^1 \leq L$, $0 \leq x^2 \leq h$. The **PI** centers c_1 , c_2 and the inter-**PI** distance d are also marked.

proteins whose extension is much larger than d :

$$U(d) \equiv \int_{\Omega} \left(\frac{\kappa}{2} H^2 + \sigma \right) dS - U_{\infty}, \quad (22)$$

where $dS \equiv \sqrt{\det g} dx^1 dx^2$ is the area element [27]. In Eq. (22), U_{∞} is the membrane potential $U(d)$ for $d \rightarrow \infty$.

We considered **PIs** with contact angles with the same or opposite orientations, see panels A and B, respectively, of Fig. 7. In addition, Fig. 8A shows the interaction potential as a function of the distance d between the two **PIs** for different values of the contact angle. Figure 8B displays the potential as a function of the contact angle of one of the two **PIs**, while the other angle is held fixed. In the Figure, the term U_{∞} in Eq. (22) has been numerically evaluated setting the two **PIs** at a distance $d = 100 r_0$.

B. Steady state with flows

In this Section, we will extend the analysis of Section III A to include the presence of flows in the membrane.

The steady state with flows is described by the PDEs [21, 29]

$$\nabla_i v^i = 0, \quad (23)$$

$$\rho v^j \nabla_j v^i = \nabla^i \sigma + \eta (-\nabla_{LB} v^i + 2K v^i), \quad (24)$$

$$\rho v^i v^j b_{ji} = -2\kappa [\nabla_i \nabla^j H + 2H(H^2 - K)] + 2\sigma H + 2\eta (\nabla^i v^j) b_{ij}, \quad (25)$$

where b the second fundamental form [27].

We will consider a geometry given by a square domain with a circular hole, the **PI**, see Fig. 9. The reference frame is taken to be that of the **PI**; this means that the flow around the **PI** is studied as if the **PI** were stationary, and the surrounding fluid were moving. Importantly, here we assume that membrane deformations fall off at a distance from the **PI** comparable to the domain size L , or larger.

Given that the square boundary removes the rotational symmetry, the PDEs (23) to (25) can no longer be reduced to a set of ODEs, and a full numerical solution is needed. We numerically solve Eqs. (23) to (25) by imposing the following BCs, see Fig. 9:

$$v^1 = v_0 \text{ on } \partial\Omega_{\square}, \quad (26)$$

$$v^2 = 0 \text{ on } \partial\Omega_{\square}, \quad (27)$$

$$v^1 = 0 \text{ on } \partial\Omega_{\square}, \quad (28)$$

$$v^2 = 0 \text{ on } \partial\Omega_{\square}, \quad (29)$$

$$\sigma = \sigma_0 \text{ on } \partial\Omega_{\square}, \quad (30)$$

$$n_i \Pi^{i1} = 0 \text{ on } \partial\Omega_{\square}, \quad (31)$$

$$n^i v_i = 0 \text{ on } \partial\Omega_{\square}, \quad (32)$$

$$\nabla_i z = t_{\square} \hat{r}_i \text{ on } \partial\Omega_{\square}, \quad (33)$$

$$n^i \nabla_i z = 0 \text{ on } \partial\Omega_{\square}, \quad (34)$$

$$z = 0 \text{ on } \partial\Omega_{\square}. \quad (35)$$

In Eq. (31), $\Pi_{ij} \equiv -\sigma g_{ij} - \eta (\nabla_i v_j + \nabla_j v_i)$ is the membrane stress tensor [21, 29]. In Eq. (33), \hat{r} is the unit radius in the $x^1 x^2$ plane relative to the **PI** center c , and we have set

$$\partial\Omega_{\square} \equiv \partial\Omega_{\square} \cup \partial\Omega_{\square} \cup \partial\Omega_{\square}. \quad (36)$$

The no-slip BCs (28) and (29) reflect the assumption that phospholipids in direct contact with the protein are immobilized due to binding interactions [41]. Equations (26) and (27) represent flow of membrane elements from $\partial\Omega_{\square}$, where the velocity field is assumed to be uniform and unperturbed by the **PI**. Equation (30) reflects the hypothesis that $\partial\Omega_{\square}$ is far enough downstream of the protein that σ matches the unperturbed, intrinsic tension of the membrane, σ_0 . Equation (32) enforces the presence of two ‘walls’ on the two sides of the boundary, through which membrane elements cannot flow. Equation (33) enforces a fixed contact angle at the **PI**, reflecting binding between membrane phospholipids and the **PI**. Equation (33) imposes that the membrane is flat at the outer boundary, according to the definition above of the length scale L . Finally,

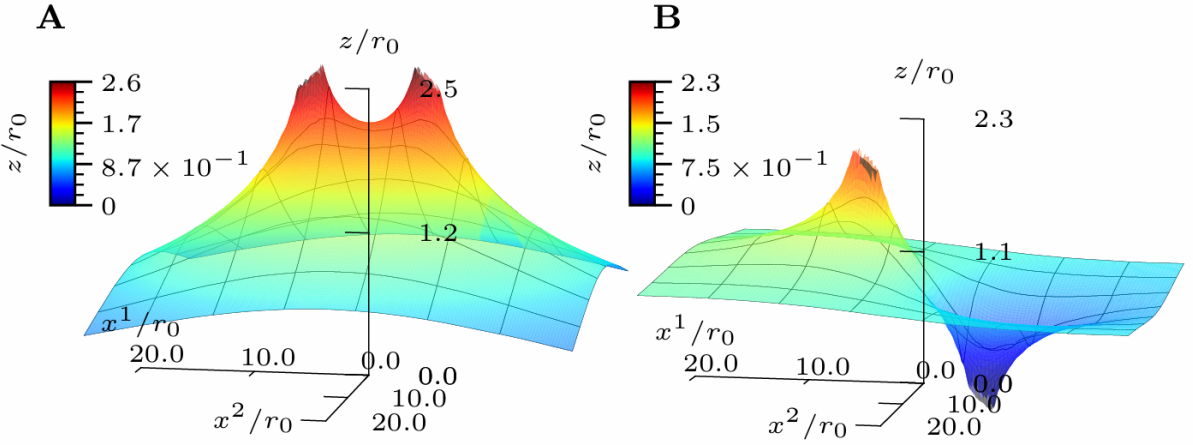


FIG. 7: Profile of a membrane with two protein inclusions in the large-deformation regime, obtained using the fluid layer finite-element software (IRENE) [28]. **A)** Two protein inclusions with contact angles given by $\tan \alpha_1 = \tan \alpha_2 = 0.6$. **B)** Same as **A**, with $\tan \alpha_1 = 0.6$ and $\tan \alpha_2 = -0.6$.

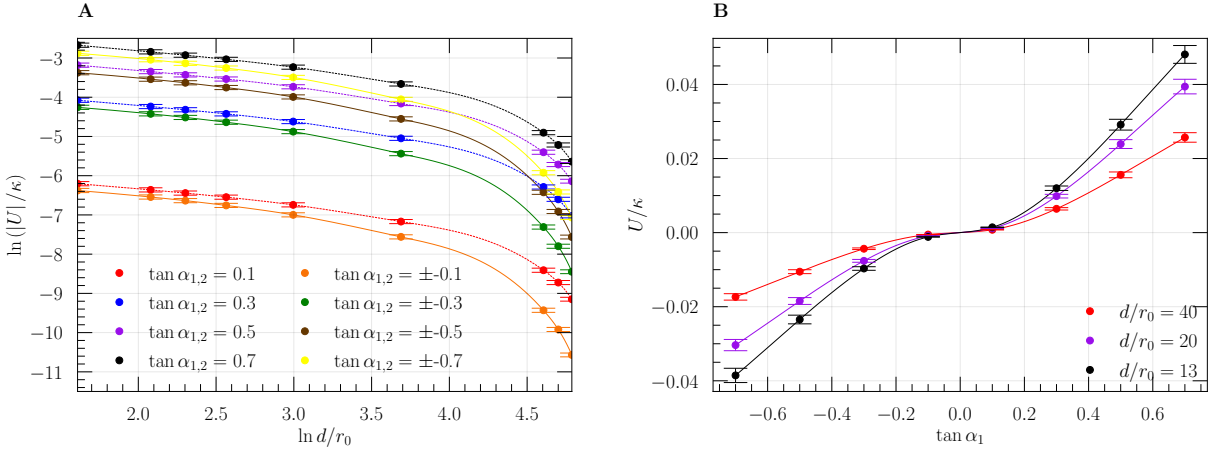


FIG. 8: Membrane-mediated interaction between two protein inclusions (PIs). **A)** Interaction potential (22) as a function of the inter-PI distance for different values of the contact angles α_1 and α_2 of the two PIs. Curves with $\tan \alpha \gtrsim 0.5$ lie in the large-deformation regime. **B)** Potential as a function of the angle of PI α_1 ; the other angle is $\alpha_2 = |\alpha_1|$.

Eq. (35) fixes the membrane height at the external boundary: This BC sets the reference height for the membrane profile, and it also reflects the assumption that membrane deformations decay at distances from the PI smaller than or equal to L .

In Fig. 10 we display the resulting numerical solution obtained by using IRENE. The parameters used in Fig. 10 are $v_0 = v_*$, where

$$v_* \equiv \frac{\kappa}{L\eta}, \quad (37)$$

$L = 10^2 r_0$, σ_0 is given in Table I, and $t_0 = -0.3$.

As shown in Fig. 11, the characteristic velocity v_* separates two different physical regimes:

- $v_0 < v_*$: The flow has no visible effect on the membrane shape, see Fig. 11A.

- $v_0 > v_*$: A membrane deformation induced by the flow appears, see Fig. 11B.

The existence of these regimes can be explained as follows. The characteristic length, or wavelength, λ , of a flow-induced deformation for a given flow velocity v , can be estimated by comparing the orders of magnitude of viscous and bending-rigidity effects. In fact, for a deformation of wavelength λ to appear, the energy cost due to viscous effects, is larger than the bending rigidity cost if $\lambda\eta v \gtrsim \kappa$. As a result, if $v \gtrsim v_*$, a flow-induced deformation

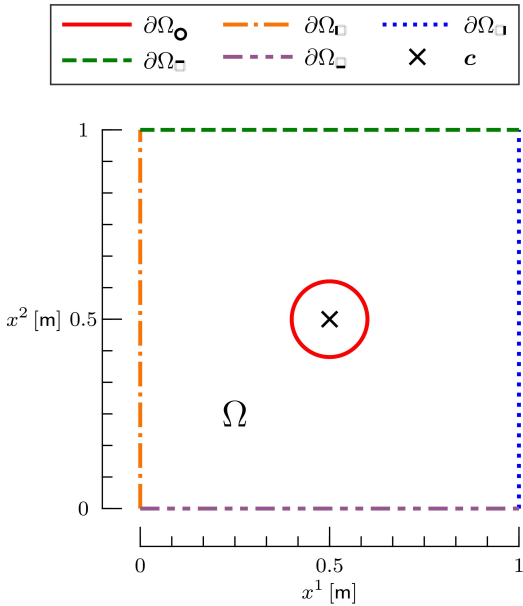


FIG. 9: Sketch of the domain Ω and its boundaries for the steady state of a membrane with a protein inclusion, in the presence of flows. The domain size is defined as in Fig. 6, the protein inclusion center (black cross) is located at $c = (L/2, L/2)$, and its radius is r_0 .

with wavelength $\sim \kappa/(v\eta) < L$ appears. On the other hand, if $v \lesssim v_*$, the flow-induced deformation wavelength would be larger than the domain size L : Given that we assumed that no membrane deformations propagate to a distance equal or larger than L from the PI, see Eqs. (34) and (35), for these velocities no deformation can appear, see Fig. 11.

IV. DISCUSSION

We have studied, by combining analytical and numerical methods, the deformations in a cell membrane induced by protein inclusions (PIs) in the large deformation (LD) regime. Our numerical analysis allows for going beyond current perturbative approaches [11–14, 16, 17, 19], which cannot describe the LD regime.

We first focused on the steady state of a lipid membrane with a single PI with spherical symmetry, where the membrane is pinned on an outer circle with radius R and the PI is located at the center. We showed the limitations of perturbative solutions by comparing them to numerically exact, finite element (FE) solutions [28], for large pro-

tein displacements or large PI contact angles, see Fig. 2. We developed an analytical solution for the shape equations in the LD regime, which assumes that the mean membrane curvature vanishes. Although this solution is only approximate, it yields a sensible, analytical expression of the membrane shape, see Fig. 4. According to this solution, a PI with a fixed contact angle has a spontaneous displacement that scales, for large R , as $\sim \ln R$, see Eq. (15). Moreover, for a straight contact angle $\alpha = \pi/2$, the spontaneous displacement remains finite, see Eq. (15). We show that the vertical component of the force exerted by the membrane on the PI—the only nonzero component due to rotational symmetry—displays a non-monotonic dependence on the vertical displacement h of the PI. This behavior is analogous to the one obtained when a point-like force is applied to a membrane [8], demonstrating that the detailed size of the PI does not affect qualitatively the force profile.

We then analyzed the force exerted by the membrane on the PI, in the LD regime. The force displays a non-monotonic dependence on the vertical displacement of the PI, reminiscent of that of a point-like force applied to a membrane [8]. We assess how this non-monotonic behavior is affected by the PI contact angle, as well as by the size of the membrane domain, see Fig. 5.

In addition, we numerically studied the membrane-mediated interaction between two PIs in the LD regime. As shown in Fig. 8A, for the values of the inter-protein distance d that we considered, the potential does not display a power-law behavior. Instead, the potential shape shows a sub-power-law decay, i.e., it decreases with d slower than a power law. This nontrivial structure is due to the complex medium which conveys the interaction—the lipid membrane [42]. Finally, Fig. 8B shows that the potential is an odd function of the PI orientation, and that two PIs with the same orientation yield a larger energy than two PIs with opposite orientations. This behavior confirms the interpretation [12] that the angle imposed by each protein can be thought of as a ‘charge’, i.e., PIs with the same and opposite orientations repel and attract each other, respectively.

In the presence of membrane flows, we identified the emergence of a characteristic velocity v_* , of the order of a few microns per second, which reflects the competition between bending and viscous forces. At low velocities, membrane flows have negligible impact on membrane shape. On the other hand, at higher velocities, flow-induced deformations appear. We provided a theoretical estimate for the critical velocity at which this deformation arises, which explains their characteristic length and aligns well

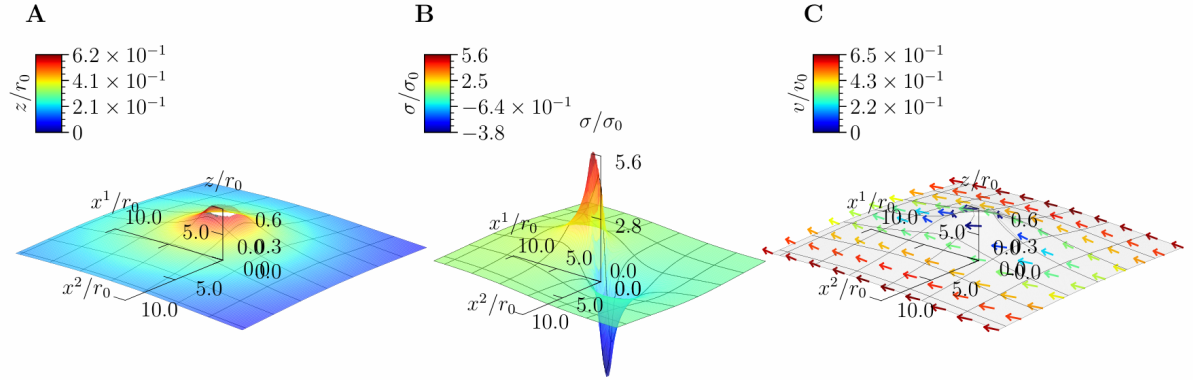


FIG. 10: Steady state with flows for an inflow velocity equal to the threshold value, $v_0 = v_*$. In **A**) Membrane shape. **B**) Membrane tension. **C**) Membrane velocity, where the velocity direction is shown by the arrows, and its norm by the color bar.

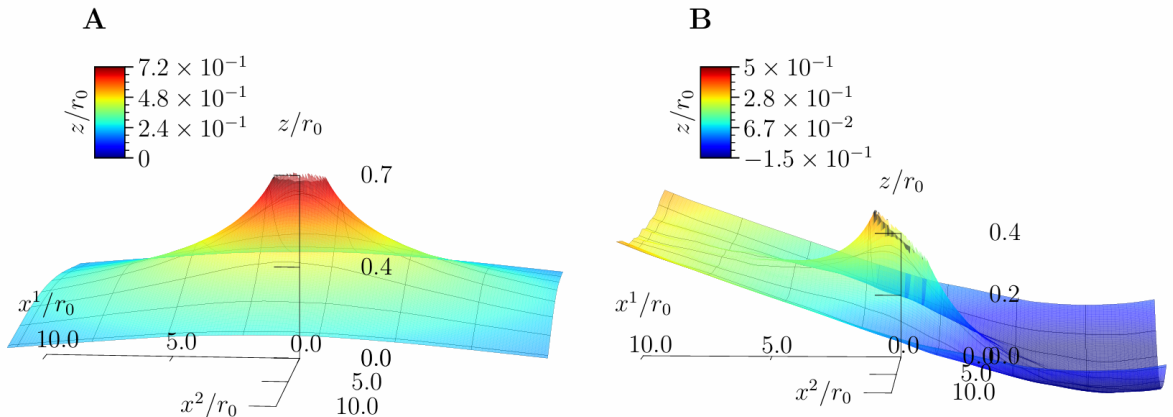


FIG. 11: Steady state with flows: membrane shape for different values of the inflow velocity. Panels **A** and **B** display the membrane shape for v_0 below and above the threshold velocity, $v_0 = 0.1 v_*$ and $v_0 = 5 v_*$, respectively.

with numerical results. The presence of this characteristic velocity scale suggests that **PIs** motion may significantly influence long-range membrane deformations and thus, for instance, membrane-mediated interactions.

An example of how flow-induced membrane deformations can influence interactions between **PIs** is given by protein clustering on giant unilamellar vesicles (**GUVs**). In this regard, we consider an example involving bacteriorhodopsin (**BR**)—the best understood ion-transport protein [43]. Multiple **BR** molecules have been incorporated and diffuse [44] on the membrane of a **GUV** [45]. A large **GUV** with a $\sim 100 \mu\text{m}$ diameter populated with $\sim 10^4$ **BRs**, yields an average inter-protein distance $d \sim 2 \mu\text{m}$. Given that the **BR** lateral diffusion coefficient of $\sim 1.2 \mu\text{m}^2/\text{sec}$, the typical values

of **BR** lateral diffusion velocity is $v \sim 2 \mu\text{m}/\text{sec}$. According to the analysis of Section III B, this implies a flow-induced membrane deformation with wavelength $\lambda \sim \kappa/(\eta v) \sim 1.5 \mu\text{m}$, comparable with the inter-protein spacing. Given that this wavelength is comparable to the spacing between **BRs**, flow-induced membrane deformations may imply a potential, significant effect on **BR** interactions and patterning on the **GUV** surface.

Future work could leverage our results to study **PI** clustering in membranes. In fact, our analysis may be extended to study systems with more than two **PIs**, examining how collective effects influence membrane deformation and forces, both with and without membrane flows. This analysis can also provide novel insights on **PI** clusters [42, 46], as well as on the effect of membrane-mediated forces on

the cluster assembly mechanisms and scaling laws. Finally, a full stability analysis of the governing equations may reveal the existence of flow-driven instabilities at larger velocities, with implications for membrane trafficking [2] and mechanosensitive processes in cells [47].

V. ACKNOWLEDGMENTS

We would like to thank P. Bassereau, D. Lacoste, P. Sens and D. Wörthmuller for useful discussions.

Appendix A: Geometrical quantities for the zero-curvature solution

By substituting Eq. (9) the definitions of the geometrical quantities [26], we obtain

$$\begin{aligned} \sqrt{\det g} &= \frac{r}{\sqrt{\psi^2 + 1}}, \\ g^{rr} &= 1 + \psi^2, \\ g^{r\theta} &= 0, \\ g^{\theta\theta} &= 1, \\ H &= \frac{1}{2} \left(\frac{\partial \psi}{\partial r} + \frac{\psi}{r} \right), \\ K &= \frac{\psi}{r} \frac{\partial \psi}{\partial r}. \end{aligned} \quad (\text{A1})$$

Appendix B: Variation of the Helfrich-Canham's energy functional

In order to find the line forces acting on the membrane boundary, we evaluate the variation of

the Helfrich energy functional [10] to linear order under a perturbation of the membrane shape of the form

$$\delta \mathbf{X} = \mathbf{N}\psi + \mathbf{e}_i\phi^i, \quad (\text{B1})$$

where \mathbf{X} is the three-dimensional position vector of the membrane surface, \mathbf{N} is its normal and \mathbf{e}_i the tangent vectors relative to the coordinate lines x^i [26–28]. Note that \mathbf{n} is a vector in three-dimensional Euclidean space, which is different from the normal n^i defined on the tangent bundle of the membrane manifold [28], see Section III A 1. Detailed calculation are presented in [26], the final

result is:

$$\begin{aligned} \delta \mathcal{H}[z] = \int_{\Omega} dS [\psi (4\kappa H^3 - 2\sigma H - 4\kappa HK) + \\ \nabla_i \phi^i (2\kappa H^2 + \sigma) + 2\kappa H \nabla^i \nabla_i \psi]. \end{aligned} \quad (\text{B2})$$

Multiple integrations by parts lead to

$$\begin{aligned} \delta \mathcal{H}[z] = \int_{\Omega} dS (4\kappa H^3 - 2H\sigma - 4\kappa HK + \\ 2\kappa \psi \nabla_i \nabla^i H) \psi + \\ \int_{\partial\Omega} dl 2\kappa [H n^i \nabla_i \psi - \psi n_i \nabla^i H + \\ + n_i \phi^i (2\kappa H^2 + \sigma)]. \end{aligned} \quad (\text{B3})$$

The terms in the integral over the boundary $\partial\Omega$ that are proportional to ψ and ϕ^i represent the inverse of the line forces acting on the membrane boundary, that is Eqs. (17) and (18) with exchanged sign.

[1] B. Alberts, R. Heald, A. Johnson, D. Morgan, M. Raff, K. Roberts, and P. Walter, *Molecular Biology of the Cell: Seventh International Student Edition with Registration Card* (WW Norton & Company, 2022).

[2] I. Bethani, S. S. Skåland, I. Dikic, and A. Acker-Palmer, Spatial organization of transmembrane receptor signalling, *EMBO J* **29**, 2677 (2010).

[3] J.-B. Manneville, P. Bassereau, D. Lévy, and J. Prost, Activity of Transmembrane Proteins Induces Magnification of Shape Fluctuations of Lipid Membranes, *Phys. Rev. Lett.* **82**, 4356 (1999).

[4] I. Koltover, J. O. Rädler, and C. R. Safinya, Membrane Mediated Attraction and Ordered Aggregation of Colloidal Particles Bound to Giant Phospholipid Vesicles, *Phys. Rev. Lett.* **82**, 1991 (1999).

[5] H. T. McMahon and J. L. Gallop, Membrane curvature and mechanisms of dynamic cell membrane remodelling, *Nature* **438**, 590 (2005).

[6] D. Marsh, Protein modulation of lipids, and vice-versa, in membranes, *Biochimica et Biophysica Acta (BBA) - Biomembranes* **1778**, 1545 (2008).

[7] F. Jülicher and U. Seifert, Shape equations for axisymmetric vesicles: A clarification, *Phys. Rev.*

E **49**, 4728 (1994).

[8] I. Derényi, F. Jülicher, and J. Prost, Formation and Interaction of Membrane Tubes, *Phys. Rev. Lett.* **88**, 238101 (2002).

[9] O.-Y. Zhong-can and W. Helfrich, Bending energy of vesicle membranes: General expressions for the first, second, and third variation of the shape energy and applications to spheres and cylinders, *Phys. Rev. A* **39**, 5280 (1989).

[10] W. Helfrich, Elastic Properties of Lipid Bilayers: Theory and Possible Experiments, *Zeitschrift für Naturforschung C* **28**, 693 (1973).

[11] M. Goulian, R. Bruinsma, and P. Pincus, Long-Range Forces in Heterogeneous Fluid Membranes, *Europhys. Lett.* **22**, 145 (1993).

[12] T. R. Weikl, M. M. Kozlov, and W. Helfrich, Interaction of Conical Membrane Inclusions: Effect of Lateral Tension, *Phys. Rev. E* **57**, 6988 (1998), [arXiv:cond-mat/9804187](https://arxiv.org/abs/cond-mat/9804187).

[13] P. G. Dommersnes, J. B. Fournier, and P. Galatola, Long-range elastic forces between membrane inclusions in spherical vesicles, *Europhys. Lett.* **42**, 233 (1998).

[14] K. Kim, J. Neu, and G. Oster, Curvature-Mediated Interactions Between Membrane Proteins, *Biophysical Journal* **75**, 2274 (1998).

[15] P. Bassereau, R. Jin, T. Baumgart, M. Deserno, R. Dimova, V. A. Frolov, P. V. Bashkirov, H. Grubmüller, R. Jahn, H. J. Risselada, L. Johannes, M. M. Kozlov, R. Lipowsky, T. J. Pucadyil, W. F. Zeno, J. C. Stachowiak, D. Stamou, A. Breuer, L. Lauritsen, C. Simon, C. Sykes, G. A. Voth, and T. R. Weikl, The 2018 biomembrane curvature and remodeling roadmap, *Journal of Physics D: Applied Physics* **51**, 343001 (2018).

[16] V. Marchenko and C. Misbah, Elastic interaction of point defects on biological membranes, *Eur. Phys. J. E* **8**, 477 (2002).

[17] D. Bartolo and J.-B. Fournier, Elastic interaction between "hard" or "soft" pointwise inclusions on biological membranes, *The European Physical Journal E - Soft Matter* **11**, 141 (2003).

[18] M. M. Mueller, M. Deserno, and J. Guven, Interface mediated interactions between particles – a geometrical approach, *Phys. Rev. E* **72**, 061407 (2005), [arXiv:cond-mat/0506019](https://arxiv.org/abs/cond-mat/0506019).

[19] M. M. Mueller, M. Deserno, and J. Guven, Geometry of surface mediated interactions, *Europhys. Lett.* **69**, 482 (2005), [arXiv:cond-mat/0409043](https://arxiv.org/abs/cond-mat/0409043).

[20] U. Seifert, K. Berndl, and R. Lipowsky, Shape transformations of vesicles: Phase diagram for spontaneous- curvature and bilayer-coupling models, *Phys. Rev. A* **44**, 1182 (1991).

[21] M. Arroyo and A. DeSimone, Relaxation dynamics of fluid membranes, *Phys. Rev. E* **79**, 031915 (2009).

[22] A. Mahapatra, D. Saintillan, and P. Rangamani, Transport Phenomena in Fluid Films with Curvature Elasticity, *Journal of Fluid Mechanics* **905**, A8 (2020), [arXiv:2001.07539 \[cond-mat\]](https://arxiv.org/abs/2001.07539).

[23] I. V. Tasso and G. C. Buscaglia, A finite element method for viscous membranes, *Computer Meth-*ods in Applied Mechanics and Engineering **255**, 226 (2013).

[24] B. Antonny, C. Burd, P. De Camilli, E. Chen, O. Daumke, K. Faelber, M. Ford, V. A. Frolov, A. Frost, J. E. Hinshaw, T. Kirchhausen, M. M. Kozlov, M. Lenz, H. H. Low, H. McMahon, C. Merrifield, T. D. Pollard, P. J. Robinson, A. Roux, and S. Schmid, Membrane fission by dynamin: What we know and what we need to know, *The EMBO Journal* **35**, 2270 (2016).

[25] C.-C. Hsiung, *A First Course in Differential Geometry* (John Wiley & Sons, New York, USA, 1981).

[26] M. Deserno, Notes on Differential Geometry, https://www.cmu.edu/biophys/deserno/pdf/diff_geom.pdf (2004).

[27] S. Marchiafava, *Appunti Di Geometria Differenziale*, Vol. I, II, III (Edizioni Nuova Cultura, 2005).

[28] D. Wörthmüller, G. Ferraro, P. Sens, and M. Castellana, IRENE: A fluid layeR finiteE-elemeNt softwarE, [http://arxiv.org/abs/2506.17827](https://arxiv.org/abs/2506.17827) (2025), [arXiv:2506.17827 \[physics\]](https://arxiv.org/abs/2506.17827).

[29] S. C. Al-Izzi, P. Sens, and M. S. Turner, Shear-Driven Instabilities of Membrane Tubes and Dynamin-Induced Scission, *Phys. Rev. Lett.* **125**, 018101 (2020).

[30] B. Alberts, A. Johnson, J. Lewis, M. Raff, K. Roberts, and P. Walter, *Molecular Biology of the Cell* (Garland Science, 2007).

[31] M. Aivaliotis, P. Samolis, E. Neofotistou, H. Remigy, A. K. Rizos, and G. Tsotis, Molecular size determination of a membrane protein in surfactants by light scattering, *Biochimica et Biophysica Acta (BBA) - Biomembranes* **1615**, 69 (2003).

[32] T. T. Hormel, S. Q. Kurihara, M. K. Brennan, M. C. Woźniak, and R. Parthasarathy, Measuring Lipid Membrane Viscosity Using Rotational and Translational Probe Diffusion, *Phys. Rev. Lett.* **112**, 188101 (2014).

[33] F. Brochard-Wyart, N. Borghi, D. Cuvelier, and P. Nassoy, Hydrodynamic narrowing of tubes extruded from cells, *Proc. Natl. Acad. Sci. U.S.A.* **103**, 7660 (2006).

[34] S. Morlot, V. Galli, M. Klein, N. Chiaruttini, J. Manzi, F. Humbert, L. Dinis, M. Lenz, G. Cappello, and A. Roux, Membrane Shape at the Edge of the Dynamin Helix Sets Location and Duration of the Fission Reaction, *Cell* **151**, 619 (2012).

[35] F. Quemeneur, J. K. Sigurdsson, M. Renner, P. J. Atzberger, P. Bassereau, and D. Lacoste, Shape matters in protein mobility within membranes, *Proc. Natl. Acad. Sci. U.S.A.* **111**, 5083 (2014).

[36] M. M. Kozlov and L. V. Chernomordik, Membrane tension and membrane fusion, *Current Opinion in Structural Biology* **33**, 61 (2015).

[37] N. C. Gauthier, T. A. Masters, and M. P. Sheetz, Mechanical feedback between membrane tension and dynamics, *Trends in Cell Biology* **22**, 527 (2012).

[38] C. M. Bender and S. A. Orszag, *Advanced Mathematical Methods for Scientists and Engineers I*

(Springer, New York, NY, 1999).

[39] R. Bruinsma and P. Pincus, Protein aggregation in membranes, *Current Opinion in Solid State and Materials Science* **1**, 401 (1996).

[40] J.-B. Fournier, Coupling between membrane tilt-difference and dilation: A new “ripple” instability and multiple crystalline inclusions phases, *Euro-physics Letters (EPL)* **43**, 725 (1998), arXiv:cond-mat/9806269.

[41] L. D. Landau and E. M. Lifschitz, *Fluid Mechanics* (Pergamon, 1987).

[42] L. Johannes, W. Pezeshkian, J. H. Ipsen, and J. C. Shillcock, Clustering on Membranes: Fluctuations and More, *Trends in Cell Biology* **28**, 405 (2018).

[43] U. Haupts, J. Tittor, and D. Oesterhelt, CLOSING IN ON BACTERIORHODOPSIN: Progress in Understanding the Molecule, *Annu. Rev. Biophys.* **28**, 367 (1999).

[44] N. Kahya, E.-I. Pécheur, W. P. De Boeij, D. A. Wiersma, and D. Hoekstra, Reconstitution of Membrane Proteins into Giant Unilamellar Vesicles via Peptide-Induced Fusion, *Biophysical Journal* **81**, 1464 (2001).

[45] P. Walde, K. Cosentino, H. Engel, and P. Stano, Giant Vesicles: Preparations and Applications, *Chem-BioChem* **11**, 848 (2010).

[46] K. Radhakrishnan, Á. Halász, M. M. McCabe, J. S. Edwards, and B. S. Wilson, Mathematical Simulation of Membrane Protein Clustering for Efficient Signal Transduction, *Ann Biomed Eng* **40**, 2307 (2012).

[47] X. Di, X. Gao, L. Peng, J. Ai, X. Jin, S. Qi, H. Li, K. Wang, and D. Luo, Cellular mechanotransduction in health and diseases: From molecular mechanism to therapeutic targets, *Sig Transduct Target Ther* **8**, 282 (2023).